JOURNAL OF MATERIALS SCIENCE **39** (2004) 3549– 3562

Review
Effect of anions on the textural and catalytic activity of titania-silica mixed oxide

S. K. SAMANTARAY, K. PARIDA*
EM & IC Department, Regional Research Laboratory (CSIR), Bhubaneswar-751 013, Orissa, India
E-mail: kmparida@yahoo.com

An attempt has been made to review and study the effect of anions (phosphate, sulfate and fluoride) on titania-silica samples. A comparative study has been made on structural characteristics and physico-chemical properties between the unmodified and anion modified titania-silica mixed oxides. The stabilisations of phase, porosity and sulphate ion at higher activation temperatures are discussed. The increase and decrease of specific surface area, acid strength and surface acid sites with respect to anions are emphasised. The effect of preparation method and conditions with specific surface area, porosity and surface acid sites are also discussed. The generation of new catalytic active sites and effect of porosity are reported towards esterification of acetic acid and mono-nitration of toluene, respectively.

1. Introduction

Now a days-chemical industry is facing challenges to reduce the use of environmentally hazardous chemicals. Central to this problem, search for a better methodology for chemical industries, has been of great interest to the scientist throughout the world. Replacement of liquid acids by solid acids is now considered as an essential element to design a cleaner process for better protection of the environment. It is reported that many kinds of binary mixed oxide systems possess higher surface acid site than single oxide [1]. Titania-silica has recently attracted much attention as its acid strength is greater than that of alumino-silicates and gives excellent result for a number of acid catalyzed reactions [2–7]. Though the actual mechanism of generation of acid sites has not yet been properly understood still, Tanabe *et al.* [8] have suggested that Brönsted sites are generated on silica riched mixed oxides, whereas according to Kung *et al.* [9] Lewis sites predominates on titania incorporated silica samples.

Modification of the single oxides with different anions like SO_4^{2-}, PO_4^{3-}, WO_4^{2-}, F^- etc. have been found to enhance the acidity and certain other physico-chemical properties of the catalyst like thermal stability, mesoporosity etc. [10–13]. However, the textural properties of these anion modified metal oxides are very poor, e.g., low surface areas and wide pore distributions. Since certain chemical processes require much stronger acid sites, it is desired to incorporate more and stronger acid sites by modifying the binary mixed oxides with anions. Very few numbers of paper have published on anion modified titania-silica mixed oxides [14–21]. Acid strength of sulfated titania-silica with respect to concentration of titania is reported [14, 15]. Lewis and Bronsted acidic sites were developed in anion modified titania-silica mixed oxides [16, 18–21] whereas the strength of the acid sites strongly depend on the method of impregnation [17].

In the present paper we have reviewed and studied the surface and textural properties of anion modified titania-silica mixed oxides and their correlation with the catalytic activity for alcohol conversion, cumene cracking/dehydrogenation, nitration of toluene and esterification of acetic acid.

2. Results and discussion

2.1. TG-DTA

The TG curves (Fig. 1a) of the unmodified and phosphate modified TiO_2-SiO_2 gels show a notable weight loss of 50% on heating TiO_2-SiO_2 mixed oxide up to 1423 K. A simple mass balance shows that the loss of weight corresponds to the quantity of reactants (water, isopropyl, butyl radicals) involved in the synthesis of TiO_2-SiO_2 gels. There is no additional weight loss in phosphate-modified TiO_2-SiO_2 mixed oxide up to 1423 K, indicating no loss of phosphate up to that temperature. There are three main domains, which can be distinguished from the DTA profiles (Fig. 1b):

- Between 293 and 523 K, a broad endothermic peak appeared, due to the loss of physisorbed water and the alcohols trapped in the porous texture.

*Author to whom all correspondence should be addressed.

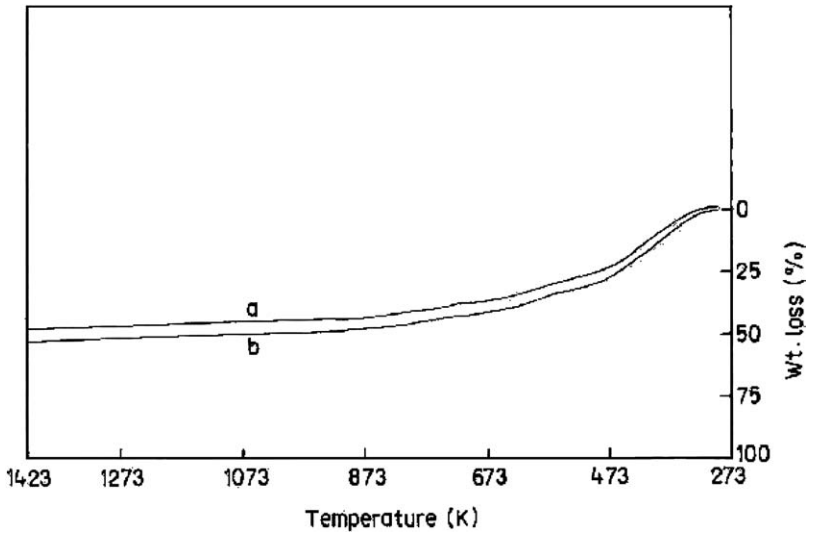

Figure 1a Thermogravimetry analysis of (a) unmodified and (b) phosphate modified TiO_2-SiO_2 samples.

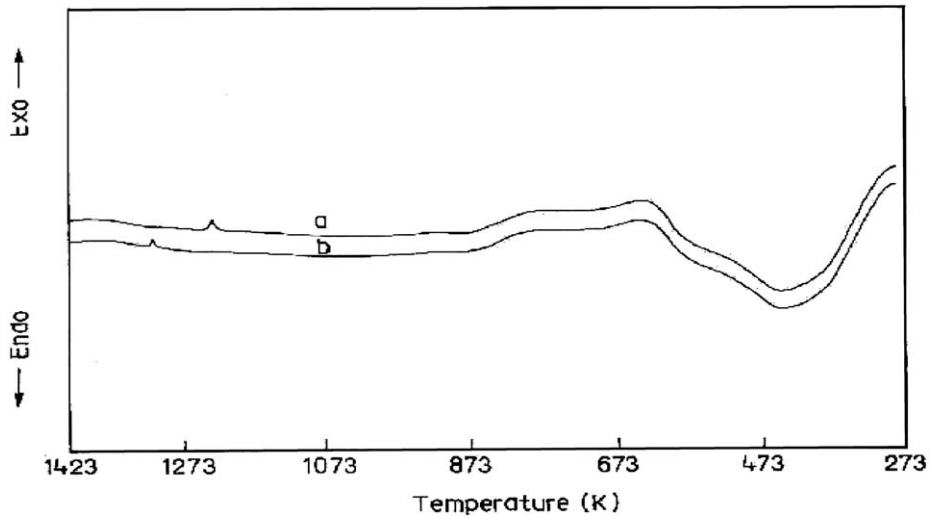

Figure 1b Differential thermal analysis of (a) unmodified and (b) phosphate modified TiO_2-SiO_2 samples.

- Between 573 and 723 K, a broad exothermic peak due to the combustion of remaining alkoxy group resulting from the incomplete hydrolysis/polycondensation reaction bound to titanium and silicon. The trapped alcohols with the porous texture may also contribute to this exothermic peak. After thermal treatment at 623 K, the sample became dark brown.
- Between 723 and 873 K, the second broad exothermic peak is probably due to a harder oxidation of the carboned residues coming from the combustion [22, 23]. Its intensity is lower than that of the first one.

An exothermic peak observed prominently in the region near (1200–1350 K) for phosphate-modified TiO_2-SiO_2 and, to a lower extent, the one for unmodified TiO_2-SiO_2 without any corresponding weight loss are very likely due to solid-state transformations (anatase to rutile phase). Its position at so high a temperature that agrees with the inhibiting effect of phosphate species on the transformation of anatase to rutile already reported [24].

Whereas, the sample containing sulfate (Fig. 2b, b) shows a weak sharp exothermic peak at 723 K attributed to the decomposition of sulfate group. But at this temperature no peak is observed in case of fluoride-modified SO_4^{2-}/TiO_2-SiO_2. There is a weak broad peak observed (Fig. 2b, c) in fluoride modified SO_4^{2-}/TiO_2-SiO_2 at 873 K. No other peak is observed after this temperature. So the sulfate group may start to decompose after 873 K in the case of fluoride-modified SO_4^{2-}/TiO_2-SiO_2.

2.2. FT-IR

The FT-IR absorption spectra of the unmodified and phosphate modified TiO_2-SiO_2 activated at 773 K (Fig. 3) shows the band at 935 cm^{-1} is attributed to the Ti—O—Si bond and the bands at 400–600, 800 and 1064 cm^{-1} are related to the Ti—O—Ti bond and the Si—O—Si bond, respectively. The bands at 800 and 1064 cm^{-1} are attributed to the symmetric and asymmetric stretching vibrations of the Si—O—Si groups, respectively [18]. It is also found that the Ti—O—Si band intensity varies with varying the method of preparation.

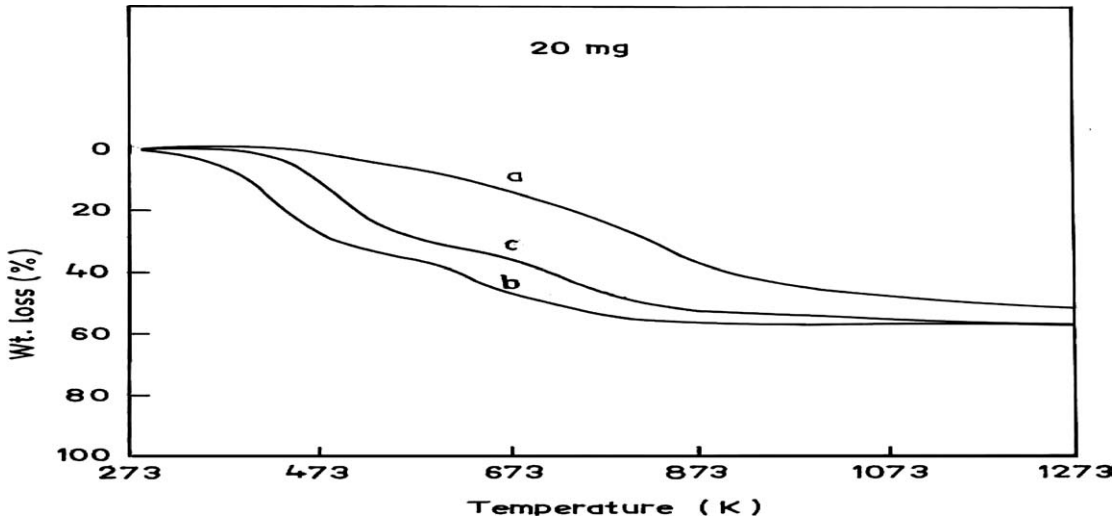

Figure 2a Thermogravimetry analysis of (a) TiO_2-SiO_2, (b) 4S/TiO_2-SiO_2(H) and (c) 2F/4S/TiO_2-SiO_2(H) samples.

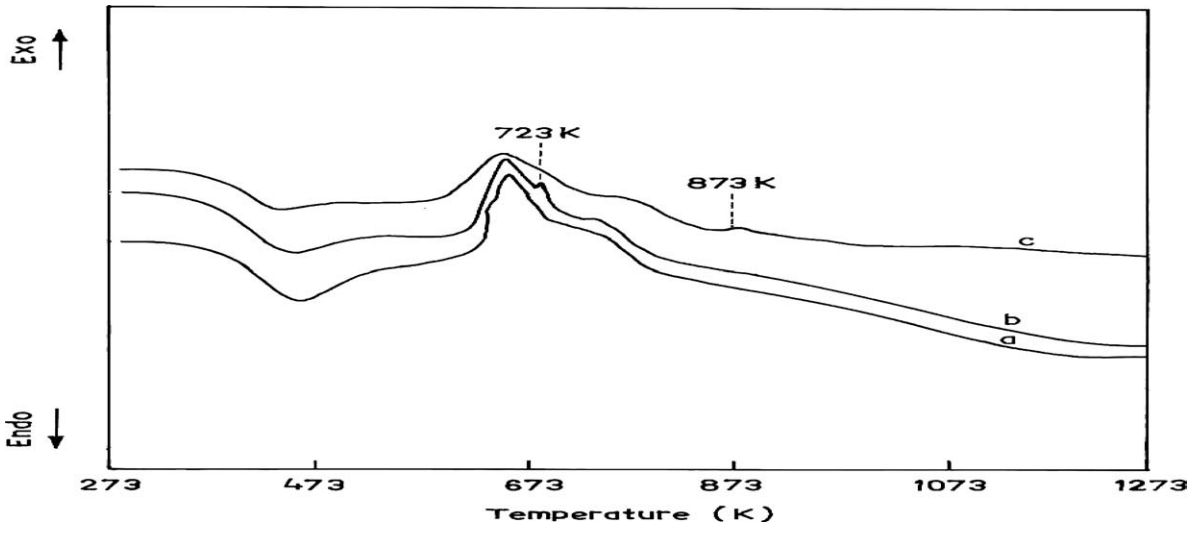

Figure 2b Differential thermal analysis of (a) TiO_2-SiO_2, (b) 4S/TiO_2-SiO_2(H), and (c) 2F/4S/TiO_2-SiO_2(H) samples.

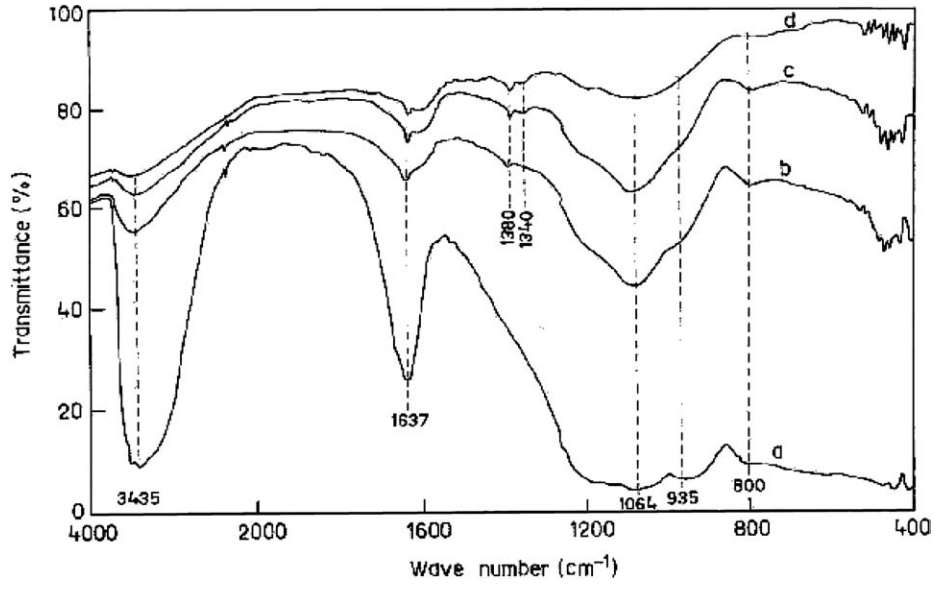

Figure 3 FT-IR spectra of (a) TiO_2-SiO_2, (b) 7.5P/TiO_2-SiO_2(H), (c) 7.5P/TiO_2-SiO_2, and (d) 7.5P/TiO_2-SiO_2(H*) samples activated at 723 K.

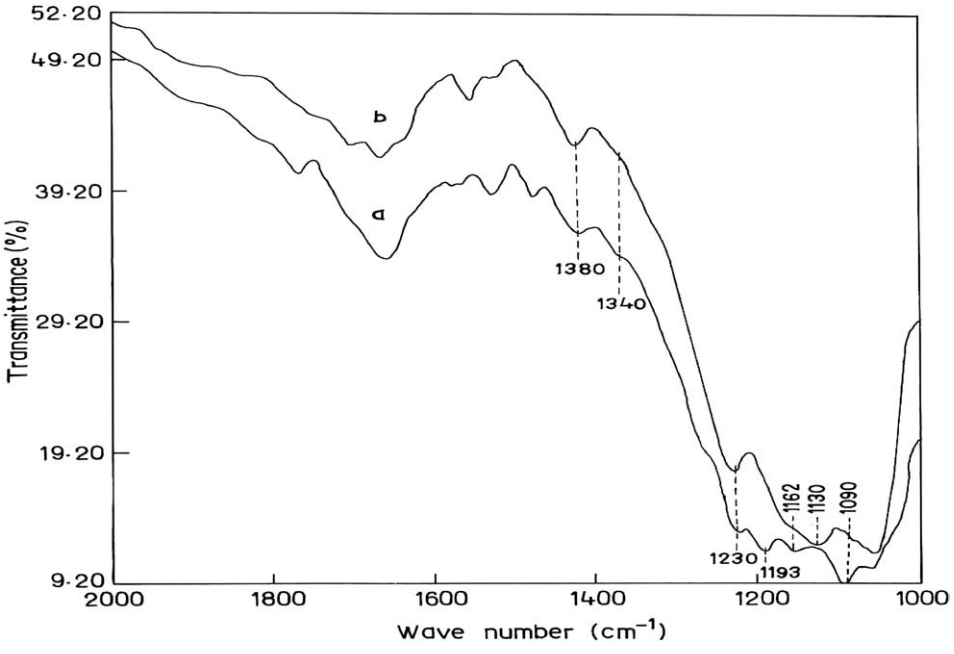

Figure 4 Resolved FT-IR spectra of 7.5P/TiO_2-SiO_2(H) samples activated at (a) 1023 and (b) 1173 K, respectively.

The Ti—O—Si band is more intense in the case of the sample prepared at pH 3 compared to the sample prepared at pH 7.

This band intensity also varies with the source of phosphate ion. The intensity of this band is more in case of phosphated TiO_2-SiO_2 (7.5 wt% PO_4^{3-}) mixed oxide, when H_3PO_4 as the source of phosphate ion, than $(NH_4)_3PO_4$. At higher activation temperatures (1023 and 1173 K), it is also observed (Fig. 4) that the Ti—O—Si band intensity decreases with increasing Ti—O—Ti and Si—O—Si bands. This is due to a reordering of the solid, which takes place by the breakage of the Ti—O—Si bond and formation of Ti—O—Ti as well as Si—O—Si bonds. This phenomenon has already been studied by Gunji *et al.* [25]. The resolved form of FT-IR spectra of phosphated TiO_2-SiO_2 mixed oxide shows (Fig. 4) a strong sharp absorption band at 1300–1400 cm^{-1} and broad bands at 1100–1250 cm^{-1}. The 1300–1400 cm^{-1} peak is the stretching frequency of P—O bond, whose order is close to two (P═O, phosphoryl groups), and the 1100–1250 cm^{-1} peaks are the characteristic frequencies of PO_4^{3-}. The broad band at 1100–1250 cm^{-1} resulted from the lowering of the symmetry in the free PO_4^{3-} (Td point group). When PO_4^{3-} is bound to the TiO_2-SiO_2 surface, the symmetry can be lowered to either C_{3V} or C_{2V} [26]. Here, the band that split into three peaks (1162, 1193 and 1230 cm^{-1}) was assigned to the bidentately bound phosphate ion (C_{2V} point group). These three bands somewhat shifted to lower wave number (Fig. 4b) when the sample is activated at 1173 K (1130, 1162 and 1230 cm^{-1}). This agrees with the position of such a fundamental band, as has been directly observed in the case of phosphated zirconia [27] and alumina [28].

The band at 1637 cm^{-1} attributed to the Si-H_2O absorption is seen on all the spectra of unmodified and phosphate-modified TiO_2-SiO_2 mixed oxide samples. The FT-IR spectra of the modified samples show sharp bands in the region 3800–3600 cm^{-1} which could be assigned to ν(OH) of free surface hydroxyl groups. A very sharp and perfectly symmetric band at 3766 cm^{-1} is seen if activation is carried out at 1173 K. At 1023 K, the spectrum shows shoulders at 3766 cm^{-1} (weak) and 3820 cm^{-1} (intense). The low frequency absorption at 3435 cm^{-1} is due to ν(OH) of internal weakly H-bonded hydroxyl groups [20, 29], while the higher frequency one at 3820 cm^{-1} has been assigned to the $\nu + \gamma$ combination of free hydroxyl groups [20, 30]. The intensity of all types of bands for OH groups seems to decrease with anion impregnation as well as on activation at higher temperature. Thus the substitution of TiO_2-SiO_2 hydroxyl groups with phosphate ion impregnation process is evident, as occurs on γ-Al_2O_3 [31] where less acidic hydroxyls groups are first removed, while hydroxyls of strong acidity are created.

Similarly, the FT-IR spectras of SO_4^{2-}, F^-/SO_4^{2-} modified and unmodified TiO_2-SiO_2 samples are shown in Fig. 5. A band is also observed at 1393 cm^{-1}, which is attributed to S═O vibration of the free sulfate groups. At 723 K, the intensity of this band is very weak (almost not found in the figure) in the case of sulfate-modified sample, while a small peak is observed in fluorinated sulfated TiO_2-SiO_2 samples. This is perhaps due to stabilisation of sulfate groups on TiO_2-SiO_2 surface above 723 K. TG-DTA analysis also supports such observations.

2.3. XRD

The powder X-ray diffraction pattern of unmodified and phosphate modified TiO_2-SiO_2 mixed oxide samples activated at different temperatures are shown in Fig. 6. It is seen from the XRD patterns that the TiO_2-SiO_2 mixed oxide sample activated at 723 K is amorphous. TiO_2 peaks are not detected in TiO_2-SiO_2 catalyst though the catalyst contains as high as 50 mol% of TiO_2(TiO_2-SiO_2). The presence of SiO_2 in TiO_2-SiO_2 obviously inhibits the growth of TiO_2 crystals and

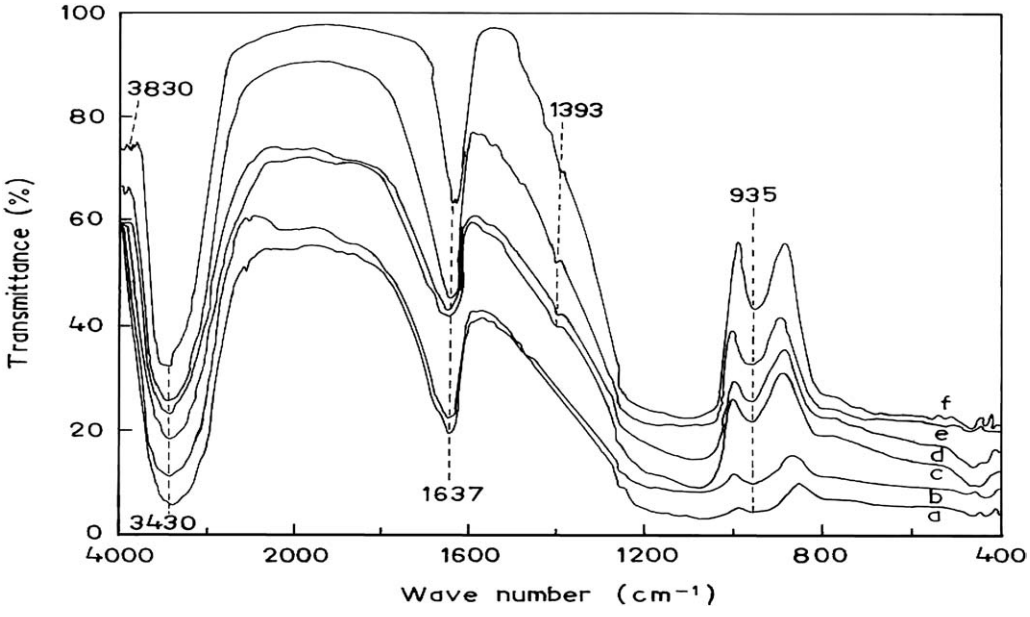

Figure 5 FT-IR spectra of (a) TiO_2-SiO_2, (b) 4S/TiO_2-SiO_2(H), (c) 0.5F/4S/TiO_2-SiO_2(H), (d) 1F/4S/TiO_2-SiO_2(H), (e) 2F/4S/TiO_2-SiO_2(H) and (f) 10F/4S/TiO_2-SiO_2(H) samples activated at 723 K.

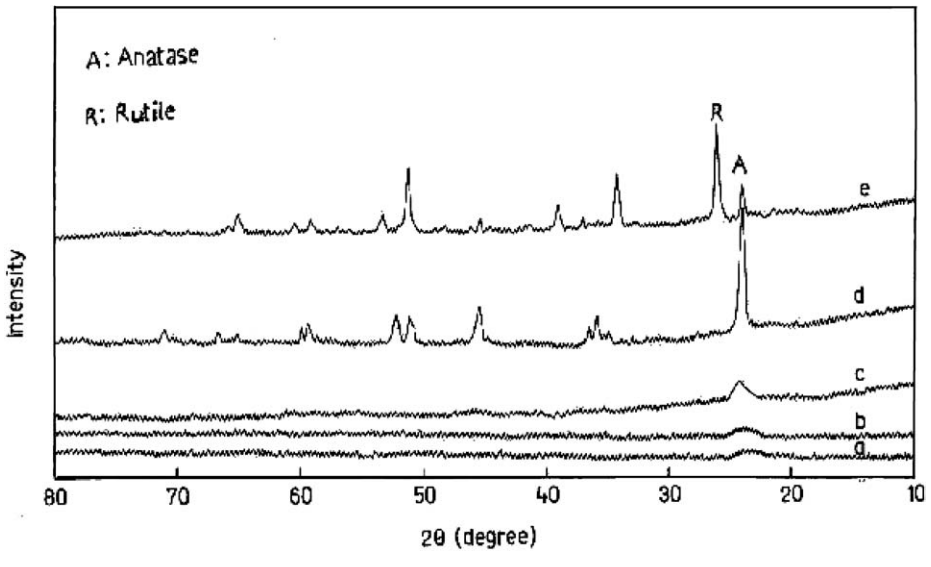

Figure 6 Powder XRD patterns of (a) TiO_2-SiO_2, 723 K and 7.5P/TiO_2-SiO_2(H) sample activated at (b) 723, (c) 923, (d) 1023 and (e) 1173 K, respectively.

results in amorphous TiO_2 [32]. However, PO_4^{3-}/TiO_2-SiO_2 shows a broad peak characteristic of TiO_2 anatase with no evidence of either rutile or silica phases. With increasing the activation temperature from 723 to 1023 K in the case of phosphate-modified TiO_2-SiO_2 samples, the intensity of diffraction lines of anatase form of TiO_2 gradually increases. But at higher activation temperature (>1173 K), both anatase and rutile forms can be identified. However, from our earlier publication [19, 20], unmodified TiO_2-SiO_2 mixed oxides shows both anatase and rutile phase of TiO_2 if activation is carried out at higher temperature than 1073 K. Such results show that phosphate could have stabilised the anatase phase up to 1173 K. TG/DTA analyses support such observations. This type of effect is also observed in SO_4^{2-} [33], PO_4^{3-} [34], and WO_3 [35] on TiO_2, α-FeOOH and ZrO_2, respectively. This result is further supported by FT-IR analysis, i.e., that a structural rearrangement of the gel occurs at higher temperatures (above 1023 K), which gives rise to Ti—O—Ti and Si—O—Si bonds.

The X-ray powder diffraction patterns of SO_4^{2-}, F^-/SO_4^{2-} modified and unmodified TiO_2-SiO_2 samples calcined at 923, 1073 and 1273 K are shown in Fig. 7. The TiO_2-SiO_2 sample is amorphous up to 1073 K and starts to crystallise after this temperature. It consists mainly of anatase phase, as revealed from the peaks at $2\theta = 26°$. When the sulfation is carried out, the crystallisation starts at lower temperature (923 K) and upon calcination at 1073 K, both the anatase and rutile allotropic forms of TiO_2 can be identified. But, when fluorination is carried out over sulfation, only the anatase phase of TiO_2 is shown at the same temperature i.e., (1073 K). At higher calcination temperature (1273 K), the intensity of diffraction lines of anatase is weak in the case of sulfated sample, compared to the case of both

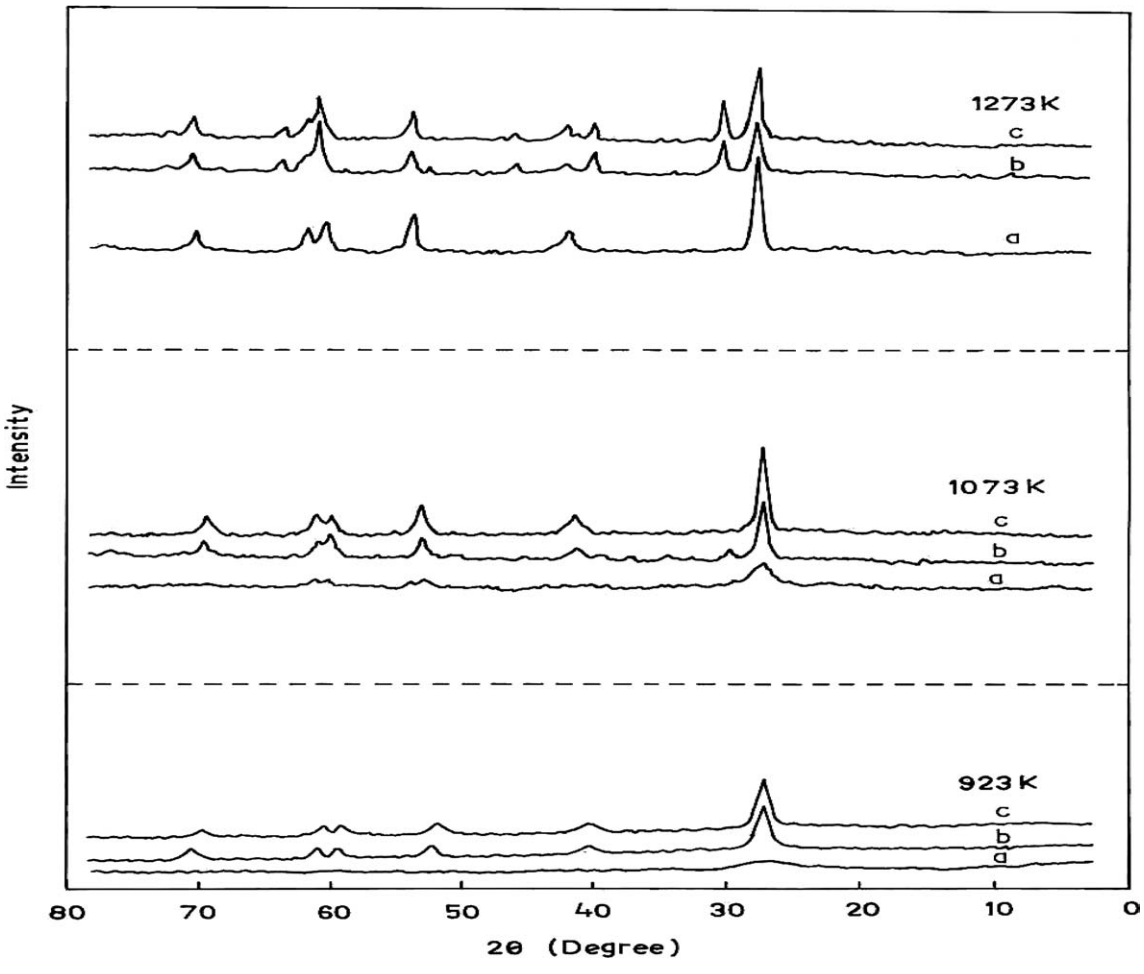

Figure 7 Powder XRD patterns of (a) TiO_2-SiO_2, (b) 4S/TiO_2-SiO_2(H) and (c) 2F/4S/TiO_2-SiO_2(H) samples activated at different temperatures.

unmodified TiO_2-SiO_2 and fluoride-modified sulfated TiO_2-SiO_2 mixed oxide.

The modifier H_2SO_4, when added to the amorphous TiO_2-SiO_2 hydrate can locate between the TiO_2-SiO_2 particles or can be adsorbed on their surface. Upon calcination at 923 K, due to decomposition of sulfate group, it may remove TiO_2 dispersed on the SiO_2 matrix, which would facilitate the crystallisation process. When both H_2SO_4 and NH_4F are added, the decomposition of sulfate group starts at higher temperature, which would stabilise the anatase phase up to 1073 K.

To develop a better understanding on the formation and crystallisation in the presence of sulfate and fluoride with sulfate ions, the average crystallite size (L) perpendicular to the 101 plane was calculated from XRD patterns of unmodified as well as modified TiO_2-SiO_2 (Fig. 8). It shows that crystallite size of TiO_2 is more in the case of sulfate than in the case of the fluoride with sulfate ion modification at 923 K. The crystallite size decreases upon higher calcination temperatures (1073 and 1273 K) in both cases, but more in the case of sulfate modification. This is due to the formation of rutile phase in case of sulfate ion modification but fluoride ion suppress the further crystallisation in case of simultaneous modification of fluoride with sulfate ions.

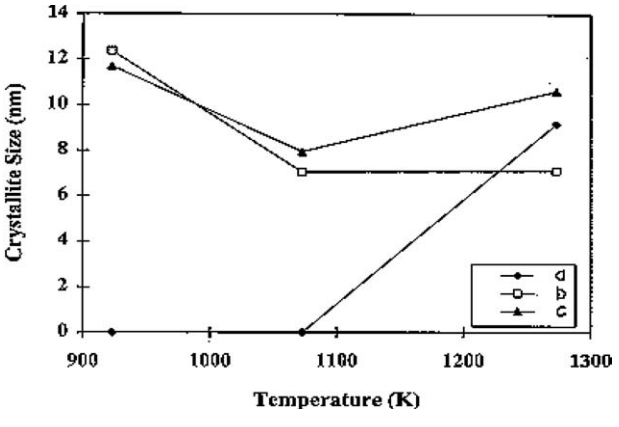

Figure 8 Average crystallite size of (a) TiO_2-SiO_2, (b) 4S/TiO_2-SiO_2(H) and (c) 2F/4S/TiO_2-SiO_2(H) samples activated at different temperatures.

2.4. Surface properties

Table I shows the BET surface area of unmodified and phosphate modified TiO_2-SiO_2 mixed oxide samples prepared by different methods. From the BET surface area measurement, it is found that surface area does not alter much by phosphate impregnation up to 7.5 wt% (341–372 m^2/g). But at higher phosphate concentration (10 wt%) the surface area decreases drastically from 372 to 261 m^2/g. It is observed that the sample prepared at pH 3 has higher surface area (377 m^2/g) than the sample prepared at pH 7 (265 m^2/g), although both the samples contain the same amount of phosphate ion (7.5 wt%). The sample containing 7.5 wt% of PO_4^{3-} (H_3PO_4 as the source of PO_4^{3-} ion) has more surface

TABLE I Textural parameters of TiO_2-SiO_2 and PO_4^{3-}/TiO_2-SiO_2 samples activated at 723 K

Sample no.	Catalysts	wt% of PO_4^{3-}	S_{BET} (m^2/g)	S_α (m^2/g)	Av. pore-radius (Å)	Pore volume
1	TiO_2-SiO_2	0.00	341	341	12.38	0.13
2	2.5P/TiO_2-SiO_2	2.90	354	353	–	–
3	5.0P/TiO_2-SiO_2	5.52	369	367	–	–
4	7.5P/TiO_2-SiO_2	8.20	372	370	4.15	0.04
5	10.0P/TiO_2-SiO_2	11.16	261	260	–	–
6	7.5P/TiO_2-SiO_2(H)	8.12	387	386	4.02	0.03
7	10.0P/TiO_2-SiO_2(H)	11.04	213	215	–	–
8	7.5P/TiO_2-SiO_2(H*)	8.04	265	266	14.24	0.14

Note: (H) and (H*) indicates H_3PO_4 impregnated on TiO_2-SiO_2 samples prepared at pH 3 and 7, respectively.

area (387 m^2/g) than the sample containing the same amount of PO_4^{3-} but obtained from a different source of phosphate ion [$(NH_4)_3PO_4$, 372 m^2/g]. The average pore radius is calculated, assuming the pores to be cylindrical, using the formula $r = 2V_p/S_p$, where r is the average pore radius, V_p is the pore volume, and S_p is the specific internal surface area of the pores measured by summing of the pore area over the whole pore system. The reverse trend is also observed for both average pore radius and total pore volume. Therefore, the presence of a low amount of phosphate ion may be responsible for the formation of porous a network. It has been shown [36, 37] that, in anion modified metal oxides, some of the hydroxyl bridges originally present in dried unactivated and unphosphated TiO_2-SiO_2 mixed oxides are replaced by the phosphate ions. On activation, the formation of oxy bonds takes place, and results in changes in the Ti—O—Si, Ti—O—Ti and Si—O—Si bond strength due to attachment of the phosphate bridges. Thus the changes in the bond strength may be responsible for the formation of porous network. However, when phosphate content increases beyond 7.5 wt%, pore blocking/formation of polyphosphate takes place due to the presence of an excess amount of phosphate ion.

N_2 adsorption-desorption isotherms of unmodified and phosphate-modified samples are of nearly the same type (Fig. 9) and can be assigned as type IV or II in the BDDT classification [38]. From the shape of the curves it can be predicted that sample prepared at pH 7 consists mainly of mesoporous material. However, the samples prepared at pH 3 are micro-mesopores. A similar observation can also be drawn from the pore size distribution curves (Fig. 10) calculated by the BJH equation [39]. Thus due to mesoporosity, samples prepared at pH 7 show a drastic decrease in surface area. The α_s-plots of the samples prepared at pH 3 show a downward deviation. However, the samples prepared at pH 7 show an upward deviation. The downward deviation reveals that these samples contain predominantly micropores, along with some mesopores, whereas an upward deviation indicates the presence of mesopores.

It is also found that (Table II) surface area does not alter much by sulfation up to 8 wt%. But at higher SO_4^{2-} wt% (10 and 15 wt%) surface area decreases slowly. However, when sulfate content increases beyond 8 wt%, pore blocking takes place due to the presence of excess of sulfate. But, with addition of a small amount of fluoride (0.5 wt%) over sulfated (4 wt%)

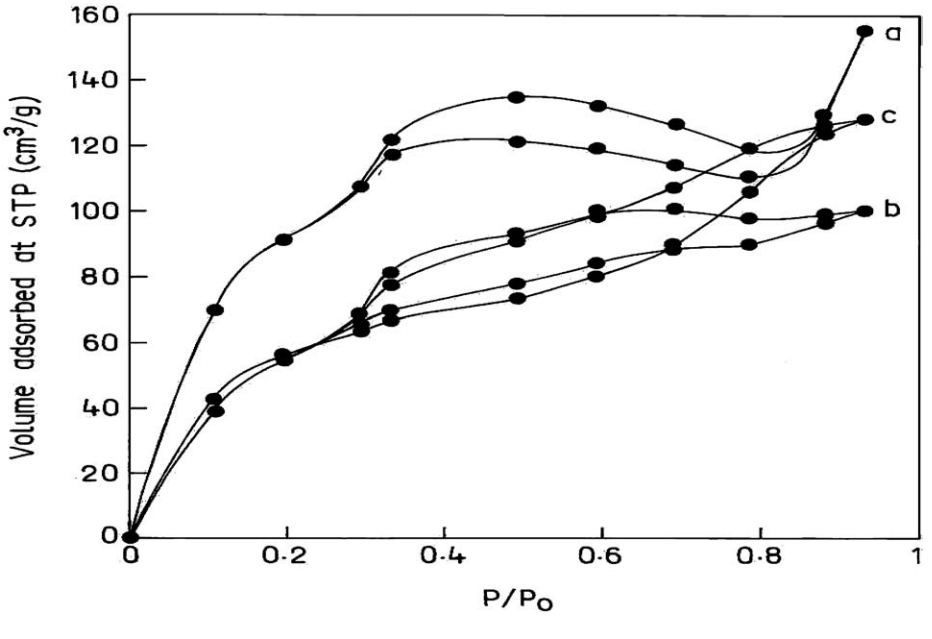

Figure 9 Nitrogen adsorption-desorption isotherm of (a) TiO_2-SiO_2, (b) 7.5P/TiO_2-SiO_2(H) and (c) 7.5P/TiO_2-SiO_2(H*) samples activated at 723 K.

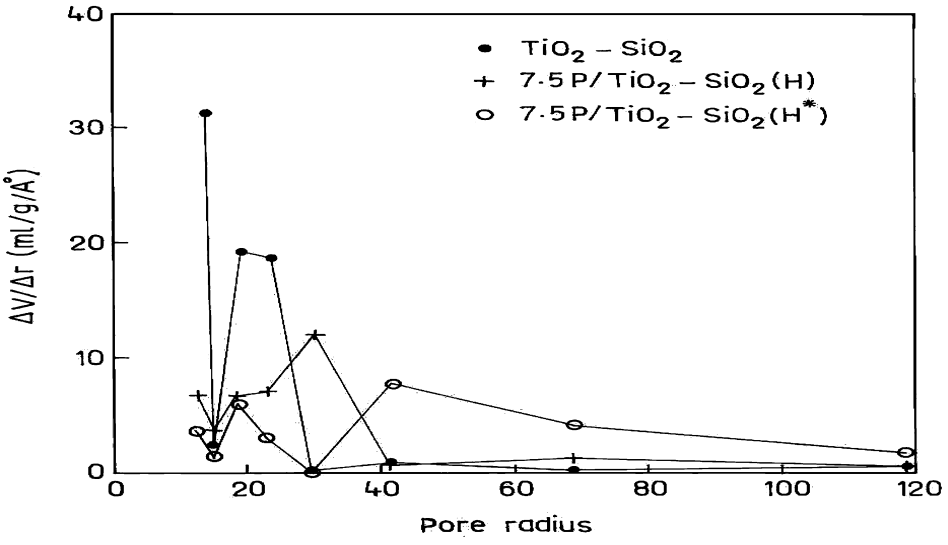

Figure 10 Distribution of pores as a function of pore radius.

TiO_2-SiO_2 calcined at 723 K decreases the surface area from 343 to 137 m^2/g (Table III). However the surface area increases by 93 m^2/g (137 to 230 m^2/g) with increase in fluoride content from 0.5 to 2.0 wt%. Again, higher fluoride loading (10.0 wt%) decreased the surface area to 144 m^2/g. An increase in surface area from 30 to 230 m^2/g was found with increase in calcination temperature from 383 to 723 K and then a decrease to 154 m^2/g at higher calcination temperature (923 K) is observed in 2.0 wt% fluoride-sulfate modified TiO_2-SiO_2 samples. The reverse order is observed in the case of pore radius. The decrease in surface area and increase in pore radius after fluorination is due to the progressive coalescence of small pores to form large pore [40]. This implies that the presence of fluoride plays a role in making the material porous. Further, the decrease in surface area beyond 10.0 wt% of fluoride and at higher calcination temperature (923 K) because of pore blocking takes place due to the presence of an excess of fluoride and sintering of the material, respectively.

The mesoporosity gradually increases with increasing fluoride content up to 2.0 wt%; however, it decreases

TABLE II Textural parameters of TiO_2-SiO_2 and sulfated TiO_2-SiO_2 samples activated at 723 K

Sample no.	Catalysts	wt% of SO_4^{2-}	S_{BET} (m^2/g)	S_α (m^2/g)	Av. pore diameter (Å)	Pore volume (ml/g)
1	TiO_2-SiO_2	0	341	341	24.76	0.172
2	$2SO_4^{2-}$/TiO_2-SiO_2(H)	2	344	340	43.34	0.134
3	$4SO_4^{2-}$/TiO_2-SiO_2(H)	4	347	345	28.42	0.113
4	$6SO_4^{2-}$/TiO_2-SiO_2(H)	6	343	335	18.9	0.2
5	$8SO_4^{2-}$/TiO_2-SiO_2(H)	8	339	340	3.76	0.14
6	$10SO_4^{2-}$/TiO_2-SiO_2(H)	10	311	296	–	0.257
7	$15SO_4^{2-}$/TiO_2-SiO_2(H)	15	292	284	15.08	0.157

Note: (H) indicates H_2SO_4 impregnated sample prepared pH 3.

TABLE III Textural parameters of SO_4^{2-}, F^-, SO_4^{2-}/F^- modified and unmodified TiO_2-SiO_2

Sample code	Activation temp. (K)	wt% of F^-	S_{BET} (m^2/g)	S_α (m^2/g)	Av. pore radius (Å)	Surface OH (meq/g)
TiO_2-SiO_2	723	0 (0)	341	341	12.38	1.5
4S/TiO_2-SiO_2(H)	723	0 (4)	347	345	14.21	1.2
2F/TiO_2-SiO_2	723	2 (0)	297	290	18.26	0.45
0.5F/4S/TiO_2-SiO_2(H)	723	0.5 (4)	137	141	16.52	0.75
1F/4S/TiO_2-SiO_2(H)	723	1.0 (4)	179	–	–	0.60
1.5F/4S/TiO_2-SiO_2(H)	723	1.5 (4)	191	–	–	0.55
2F/4S/TiO_2-SiO_2(H)	723	2.0 (4)	230	232	26.42	0.25
10F/4S/TiO_2-SiO_2(H)	723	10.0 (4)	144	–	–	0.25
2F/4S/TiO_2-SiO_2(H)	383	2.0 (4)	30	–	–	0.55
2F/4S/TiO_2-SiO_2(H)	623	2.0 (4)	53	51	29.97	0.30
2F/4S/TiO_2-SiO_2(H)	823	2.0 (4)	189	–	–	0.20
2F/4S/TiO_2-SiO_2(H)	923	2.0 (4)	154	–	–	0.15

Note: (H) indicates H_2SO_4 impregnated sample prepared at pH 3. Figures in the parentheses are the wt% of SO_4^{2-}. 2F, 4S etc. are represents loading (wt%) of fluoride and sulfate, respectively during the impregnation process.

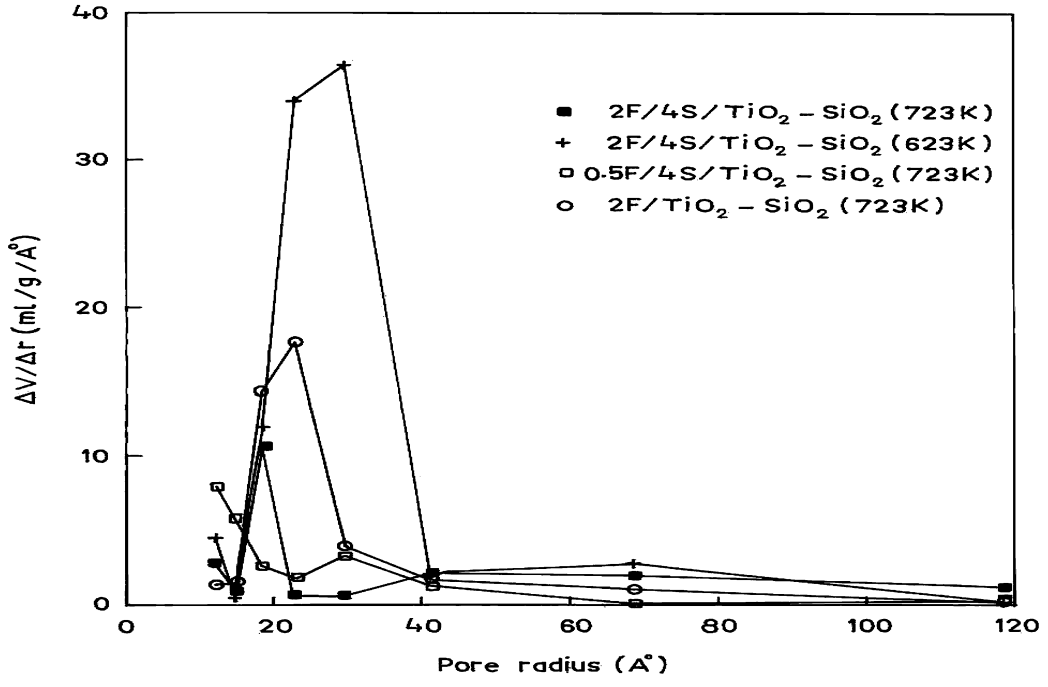

Figure 11 Distribution of pores as a function of pore radius.

with calcination temperatures (Fig. 11). The specific surface area S_α was also calculated from the slope of the straight line passing through the origin of the α_s-plot (v_a vs. α_s) using the formula $S_\alpha = 2.645\times$ slope of the text line. The surface areas S_α from the α_s-plot are very similar to those from the S_{BET} method (Table II).

The phosphate concentrations of the samples activated at 723 K are shown in Table I. The phosphate concentration in samples activated at 773 K is higher than the corresponding amount added during preparation. This is due to the loss of water (dehydration) and alcohol (adsorbed solvent in course of preparation of catalyst) during activation. Similar types of observation were also reported earlier by Pattnayak *et al.* [41].

Whereas, the calcination temperature has a dominating role on the sulfate content of both the series of samples (Table IV). Calcination of samples up to 623 K enhances the sulfate content and thereafter decreases with further increase in calcination temperature. However, the decrease in sulfate content after 723 K of calcination is more pronounced in case of SO_4^{2-}/TiO_2-SiO_2 than fluoride-modified SO_4^{2-}/TiO_2-SiO_2. A regular increase in sulfate content (wt%) up to 623 K of calcination may be attributed to loss of water (dehydration) and alcohol (adsorbed solvent in course of preparation of catalyst) as evident from TG analysis. With increase in calcination temperature (beyond 623 K) the strongly bonded sulfate group start decomposing at 723 and 923 K in case of SO_4^{2-}/TiO_2-SiO_2 and fluoride-modified SO_4^{2-}/TiO_2-SiO_2, respectively. The decomposition of sulfate at higher calcination temperature on fluoride-modified SO_4^{2-}/TiO_2-SiO_2 than SO_4^{2-}/TiO_2-SiO_2 is of interesting. The presence of fluoride might be inhibiting the loss of sulfate at higher temperature by blocking its escape from the surface.

The surface hydroxyl groups determined titrimetrically are shown in Table III. The concentration of OH groups decreases with sulfate as well as with fluoride loading up to 2.0 wt% and levels off with further increase in loading. This result is also supported by FT-IR analysis. Thus fluoride loading can be considered as monolayer coverage on the sulfated TiO_2-SiO_2 support from the fact that, in supported catalysts, the monolayer is formed by a strong chemical interaction between the OH groups of the supported surface and the supported metal oxide precursors present in the impregnating solution [42]. It may be inferred that the drop in the surface concentration of OH groups upon deposition of fluoride ions and then its leveling off at and beyond a certain loading (2.0 wt%) provide evidence for interaction between surface OH groups of the sulfated TiO_2-SiO_2 support and the active fluoride species until the completion of the monolayer. This result is confirmed by the increase in surface area up to 2.0 wt% fluoride impregnation, then a decrease on further loading.

TABLE IV The sulfate content (wt%) of different samples under investigation

T (K)	383	623	723	823	923
4S/TiO_2-SiO_2	3.97	5.17	3.22	1.31	0.23
2F/4S/TiO_2-SiO_2	3.98	5.05	4.79	3.20	2.35

Note: 4S/TiO_2-SiO_2 and 2F/4S/TiO_2-SiO_2 represents 4 wt% of SO_4^{2-}/TiO_2-SiO_2 and 2 wt% of fluoride-modified 4 wt% SO_4^{2-}/TiO_2-SiO_2, respectively.

2.5. Acid strength

Table V shows that the Hammett acidity function of 7.5P/TiO_2-SiO_2 is ≥ -13.16, whereas for TiO_2-SiO_2 it is ≥ -8.2. These results mean that the weak acid sites of unmodified catalyst are converted into strong acid sites by means of anion modification. Acids stronger than $H_o = -11.93$, which corresponds to the acid strength of 100% H_2SO_4, are known as super acids [12].

TABLE V Acid strength and surface acid sites of the TiO_2-SiO_2 and PO_4^{3-}/TiO_2-SiO_2 samples activated at 723 K

	PK_a value of indicators				
Catalysts	−8.2	−12.4	−13.16	−14.52	−3.0 (μmol/g)
TiO_2-SiO_2	+	−	−	−	210
2.5P/TiO_2-SiO_2	+	+	±	−	322
5.0P/TiO_2-SiO_2	+	+	±	−	346
7.5P/TiO_2-SiO_2	+	+	+	−	372
10.0P/TiO_2-SiO_2	+	+	±	−	332
7.5P/TiO_2-SiO_2(H)	+	+	+	±	405
7.5P/TiO_2-SiO_2(H*)	+	+	±	−	380

Note: (H) and (H*) indicates H_3PO_4 impregnated on TiO_2-SiO_2 sample prepared at pH 3 and 7, respectively.

So, 7.5P/TiO_2-SiO_2 acts as a solid super acid catalyst. The increase in acid strength in the modified catalyst is attributed to the double bond nature of P=O, which strengthens the acid sites by the inductive effect [43].

Whereas the Hammett acidity function of $4SO_4^{2-}$/TiO_2-SiO_2 is <-14.52 and for TiO_2-SiO_2 it is <-11.35 (Table VI).

It is also seen that (Table VII) the Hammett acidity function of 2F/4S/TiO_2-SiO_2 is −16.04, whereas it is >-8.2, >-12.7 and <-14.52 for TiO_2-SiO_2, 2F/TiO_2-SiO_2 and 4S/TiO_2-SiO_2, respectively. The acid strength of unmodified TiO_2-SiO_2 is less than that of the sulfate as well as that of fluoride-modified TiO_2-SiO_2. Further increase of acid strength with fluoride impregnation over SO_4^{2-}/TiO_2-SiO_2 in case of 2F/4S/TiO_2-SiO_2 is due to the simultaneous inductive effect of S=O and gem-fluoride ions.

2.6. Surface acid sites

The acid sites of unmodified and phosphate-modified TiO_2-SiO_2 mixed oxide catalysts after being activated at 723 K for 4 h were determined by titrating the solid suspended in benzene against *n*-butyl amine using dicinnamalacetone indicator, as reported in Table V. It is observed that the phosphate-modified catalysts have much more acidity than the unmodified catalyst. When one increases the PO_4^{3-} loading up to 7.5 wt%, the acidity gradually increases (322 to 372 μmol/g); thereafter it decreases to 322 μmol/g on further addition. The initial increase in surface acidity, with an increase in phosphate loading up to 7.5 wt%, may be due to phosphate monolayer formation. The decrease in the surface acidity at high phosphate concentration (10 wt%) is probably due to formation of polyphosphate, which decreases the number of Brönsted acid sites and consequently the total number of acid sites [36]. It is also observed that phosphated sample prepared using H_3PO_4 exhibit higher acidity (405 μmol/g) compared to the samples prepared using $(NH_4)_3PO_4$ (372 μmol/g) when the same amount (7.5 wt%) of phosphate was impregnated. Similarly, samples prepared at pH 3 exhibit higher acidity (405 μmol/g) than the samples prepared at pH 7 (380 μmol/g). It is reasonable to assume that, during the preparation procedure, the aqueous phosphoric acid protonates all types of hydroxyls (TiO_2-SiO_2) by an acid-base reaction. However, phosphate of ammonium phosphate by solid-solid kneading method undergoes interaction with all types of basic hydroxyls to a smaller extent, resulting in less acidity compared to phosphate of phosphoric acid by aqueous impregnation method. Similar observations have been reported earlier in the cases of SO_4^{2-} [44] and PO_4^{3-} [45] on alumina. It is observed (Table VI) that the sulfate modified catalysts have much more acidity than the unmodified as well as phosphate modified catalyst. The acidity gradually increases (475 to 638 μmol/g) by increasing the SO_4^{2-} loading up to 8.0 wt% and decreases thereafter to 386 μmol/g. It is also observed (Table VII) that the fluoride-sulfate modified TiO_2-SiO_2 mixed oxide

TABLE VI Acid strength and surface acid sites of TiO_2-SiO_2 and SO_4^{2-}/TiO_2-SiO_2 activated at 723 K by Hammett indicator method

Catalyst	+3.3[a]	−5.6[a]	−8.2[a]	−11.3[a]	−11.9[a]	−12.7[a]	−14.5[a]	−3.0 (μmol/g)
TiO_2-SiO_2	+	+	+	±	−	−	−	210
$2SO_4^{2-}$/TiO_2-SiO_2(H)	+	+	+	+	±	−	−	475
$4SO_4^{2-}$/TiO_2-SiO_2(H)	+	+	+	+	+	+	±	592
$6SO_4^{2-}$/TiO_2-SiO_2(H)	+	+	+	+	±	−	−	610
$8SO_4^{2-}$/TiO_2-SiO_2(H)	+	+	+	+	±	−	−	638
$10SO_4^{2-}$/TiO_2-SiO_2(H)	+	+	+	+	±	−	−	386
$15SO_4^{2-}$/TiO_2-SiO_2(H)	+	+	+	−	−	−	−	345

Note: [a]Indicate indicators with different pK_a values. (H) indicates H_2SO_4 impregnated sample prepared at pH 3.

TABLE VII Acid strength and surface acid sites of unmodified and modified catalysts activated at 723 K by Hammett indicator method

Hammett indicators	pK_a value of indicators	TiO_2-SiO_2	2F/TiO_2-SiO_2	4S/TiO_2-SiO_2(H)	2F/4S/TiO_2-SiO_2(H)
Anthraquinone	−8.2	+	+	+	+
Nitrobenzene	−12.4	−	+	+	+
m-nitrochlorobenzene	−13.16	−	−	+	+
2,4-dinitrotoluene	−14.52	−	−	±	+
1,3,5-trinitrotoluene	−16.04	−	−	−	+
Dicinnamalacetone	−3.0 (μmol/g)	210	435	592	715

Note: (H) indicates H_2SO_4 impregnated sample prepared at pH 3.

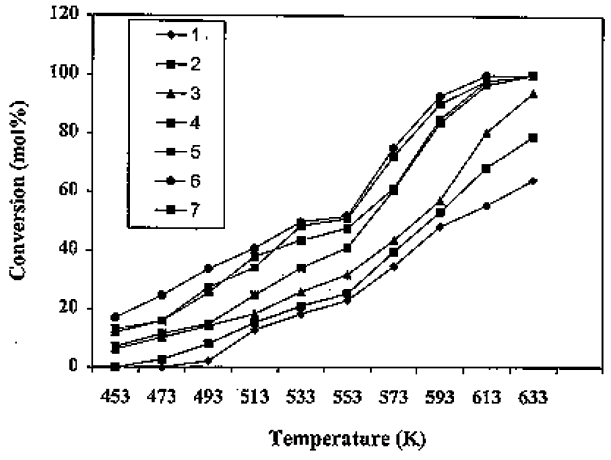

Figure 12 Conversion of 2-propanol as a function of temperature over different TiO_2-SiO_2 samples. Number refers to sample numbers (c.f. Table I).

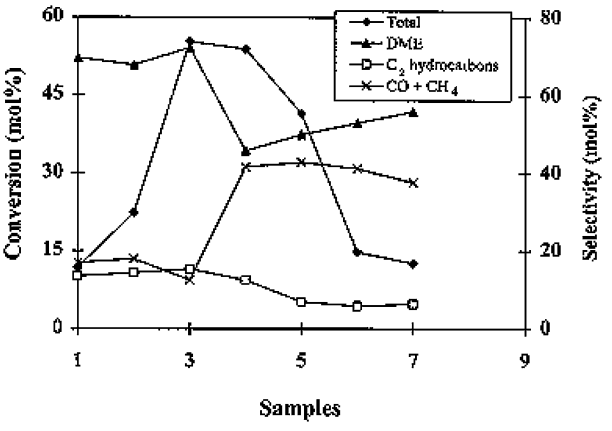

Figure 13 Selectivity of different products from methanol conversion at 723 K over different TiO_2-SiO_2 samples. Number refers to sample numbers (c.f. Table I).

sample has more acidity (715 μmol/g) compared to sulfate, fluoride modified as well as unmodified TiO_2-SiO_2 mixed oxide sample. The more acidity in case of $2F^-/4SO_4^{2-}/TiO_2$-SiO_2 (H) is due to simultaneous effect of sulfate as well as fluoride group.

2.7. Catalytic activities

Conversion of 2-propanol over acidic catalysts produces propene and isopropyl ether as the major product while acetone is the major products over catalyst containing basic and redox sites. Fig. 12 shows that transformation of 2-propanol increases with increase in sulfate content up to 10 wt% and thereafter it decreases. From the product analysis we found that propene is the major product however isopropyl ether (<2 mol%) and acetone (<2 mol%) are also formed as the minor products. Formation of acetone suggests that all the catalysts contain insufficient number of basic and redox sites [46]. As the basicity of 2-propanol is higher than methanol, it can give olefin even on weak acid sites, whereas methanol gives olefin only on strong acid sites. So the observed variation in the rate of propene formation with increase in sulfate content may be due to the increase in the number of available weak acid sites.

It has also been reported earlier [16] that sulfation of titania-silica increases the Lewis acidity of the catalyst. To differentiate between the strong and weak acid sites of the catalyst, methanol conversion was carried out. Over all the catalysts, both dimethyl ether (DME) and C_2^+ hydrocarbons are the dehydration products (Fig. 13). In addition to both of these products, CO and CH_4 is the decomposition product of DME [47], particularly at higher reaction temperatures. From Fig. 13, it is clear that dimethyl ether (DME) is the predominant product. Among all the samples, $4SO_4^{2-}/TiO_2$-SiO_2 shows highest selectivity towards C_2^+ hydrocarbons (16 mol%). But as a whole, all the samples showed low selectivity towards the C_2^+ hydrocarbons which indicates that the strengths of the major acid sites are not enough for the methanol conversion to C_2^+ hydrocarbons.

In methanol conversion reaction, the selectivity of the products are represented by their corresponding optimum performance envelope (OPE) curves (Fig. 14). These values are obtained by plotting the fractional conversion (X) of a particular product against the total conversion (X_t). This is obtained by varying catalyst to alcohol ratio (w/w) as described by Ko and Wojciechowski [48]. The OPE curves represent the conversion selectivity behaviour of active sites present on a catalyst and whose slope at the origin represents the initial selectivity for those products. For obtaining the product distribution as a function of the conversion, we have included experiments performed by varying the weight of the catalyst, so that conversion as high as 50–60 mol% can be achieved. From Fig. 14, it is observed that both DME and C_2^+ hydrocarbons are present from the onset of the reaction, which indicates that both of these are primary dehydration products. There is some marked downward deviation in the case of DME plots indicates the instability of the product. At the same time, an upward deviation is marked in the C_2^+ hydrocarbon plots. It means that DME further dehydrates to C_2^+ hydrocarbons in a secondary reaction at higher reaction temperature. All other catalysts also show nearly similar behaviour. Thus the formation of

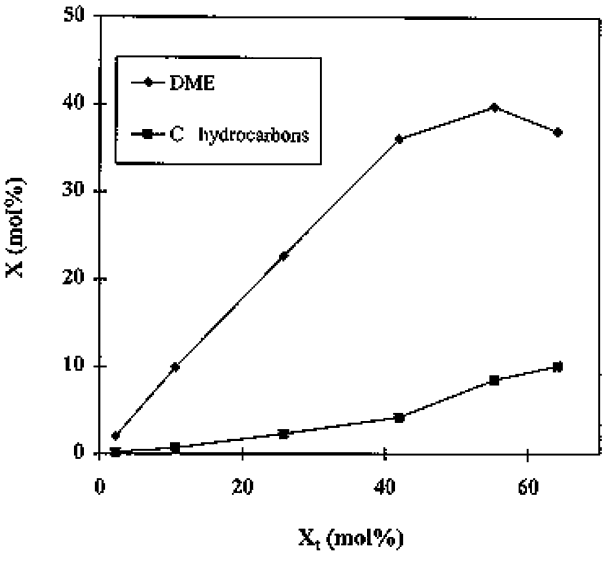

Figure 14 OPE curve for methanol conversion to dimethyl ether (DME) and C_2^+ hydrocarbons at 523 K.

TABLE VIII Cumene cracking/dehydrogenation over modified TiO_2-SiO_2 activated at 723 K at different temperatures

Reaction temp. (K)	TiO_2-SiO_2	2F/TiO_2-SiO_2	4S/TiO_2-SiO_2(H)	0.5F/4S/TiO_2-SiO_2(H)	2F/4S/TiO_2-SiO_2(H)
473	0	0	0	6.3 (1.1)	12.1 (1.37)
500	0	0	0	10.5 (1.33)	14.6 (1.43)
523	0	1.3 (1.16)	9.2 (0.12)	22.8 (1.53)	28.2 (1.76)
573	7.36 (6.36)	9.4 (2.1)	11.11 (0.121)	31.1 (1.8)	37.7 (1.96)
623	28.25 (22.54)	29.0 (2.22)	29.86 (1.87)	43.3 (2.25)	54.1 (2.86)

Note: (H) indicates H_2SO_4 impregnated sample prepared at pH 3. Figures in parentheses are the ratio of benzene to α-methyl styrene in the product.

C_2^+ hydrocarbons on TiO_2-SiO_2 and SO_4^{2-}/TiO_2-SiO_2 is a combination of parallel and consecutive (primary and secondary) reactions.

On all the acid catalysts, cumene conversion resulted in dehydrogenation as well as cracking products. α-methylstyrene is the dehydrogenation product, whereas benzene and propene are the cracking products. Table VIII represents the conversion and selectivity of different products obtained from dehydrogenation and cracking of cumene. The cumene conversion is maximum over $4SO_4^{2-}$/TiO_2-SiO_2 (64%). It is also observed that cracking products are maximum over TiO_2-SiO_2 at all temperature indicating the presence of more Bronsted acid site [49]. This cracking activity gradually decreases with varying SO_4^{2-} wt%. But the dehydrogenation product (α-methyl styrene) gradually increases with sulfation. This means that all SO_4^{2-}/TiO_2-SiO_2 possess higher number of lewis sites. Among all the sulfated samples, $4SO_4^{2-}$/TiO_2-SiO_2 showed the highest rate of reaction. Probably the increase in acid strength in case of sulfated catalysts is mainly due to the increase in number of Lewis acid sites, which facilitates the dehydrogenation reaction.

However, this cracking product increases with varying fluoride wt% over sulfated TiO_2-SiO_2 (Table VIII). It is generally accepted that cumene cracking proceeds over Bronsted sites [50]. In the mechanism, the first step is protonation of the ring of cumene, at the point of attachment of the substituents, on Bronsted acid sites, followed by cleavage of the ring-side chain bond to generate benzene and propylene. However, the formation of α-methyl styrene probably results from a free radical mechanism (over lower acid site) of cumene decomposition initiated by dehydrogenation centres [51]. This means that sulfate impregnation increases the number of Lewis acid sites but fluoride loading over sulfated TiO_2-SiO_2 probably increases the strength of Bronsted acid sites, which facilitates the cracking reaction.

Catalytic outcomes of nitration reaction of toluene are presented in Table IX. It is observed that the yield of mono-nitro toluene in the case of phosphate-modified TiO_2-SiO_2 mixed oxide is more than in the case of the unmodified TiO_2-SiO_2 catalyst. If one increases the wt% of PO_4^{3-} up to 7.5, the yield of the reaction does not increase so much. However, with higher phosphate concentration (10 wt%), the yield decreases drastically. Comparing the TiO_2-SiO_2 mixed oxide samples with the same amount of phosphate ion but different sources of the ion [H_3PO_4 and $(NH_4)_3PO_4$], one sees that the yield of mono-nitro product more or less remained the same, but the P/O ratios are different. A sample prepared from H_3PO_4 ion has more para selectivity (P/O = 2.19) than that of the sample prepared from $(NH_4)_3PO_4$ (P/O = 1.96). The same trend is also observed in case of TiO_2-SiO_2 mixed oxide samples prepared by different methods. TiO_2-SiO_2 mixed oxide samples prepared at pH 7 (impregnated with 7.5 wt% of phosphate using H_3PO_4 as the source of PO_4^{3-} ion) have less para selectivity (P/O = 1.57) than the samples prepared at pH 3 (P/O = 2.19) with the same concentration and source of phosphate ion.

TABLE IX Catalytic activity of the TiO_2-$SiO_2$and PO_4^{3-}/TiO_2-SiO_2 samples activated at 723 K towards mono-nitration of toluene

Catalysts	Yield (%)	Selectivity (%)			P/O
		Ortho (O)	Meta (M)	Para (P)	
TiO_2-SiO_2	58	36	1	63	1.75
2.5P/TiO_2-SiO_2	81	30	1	69	2.30
5.0P/TiO_2-SiO_2	82	32	1	67	2.09
7.5P/TiO_2-SiO_2	83	33	2	65	1.96
10.0P/TiO_2-SiO_2	68	35	2	63	1.80
7.5P/TiO_2-SiO_2(H)	89	31	1	68	2.19
10.0P/TiO_2-SiO_2(H)	59	35	2	63	1.80
7.5P/TiO_2-SiO_2(H*)	78	38	2	60	1.57

Note: (H) and (H*) indicates H_3PO_4 impregnated on TiO_2-SiO_2 sample prepared at pH 3 and 7, respectively.

The mechanism of nitration reaction involves electrophilic attack on the aromatic rings by the nitronium ion, NO_2^+. Bronsted acid sites are responsible for the generation of NO_2^+ ion from nitric acid, whereas Lewis acid sites are responsible for the selectivity to para product [52, 53]. The earlier work [54] emphasises the activity, yield and selectivity of the catalyst as a function of acidity of the material. However, our observation shows that the selectivity to para product decreases with increase in porosity of the material, which was also reported earlier by Kwok *et al.* [55] on zeolite catalyst (i.e., the higher the porosity, the lower the selectivity to para product). This observation is reflected on samples prepared using $(NH_4)_3PO_4$ as the source of phosphate ion and TiO_2-SiO_2 prepared at pH 7. In this case, though the porosity increases, the selectivity to para product is less compared to the samples prepared at pH 3 and H_3PO_4 as the source of phosphate ion, with almost negligible change in acidic properties.

Esterification is an acid-catalysed reaction. The reaction of acetic acid and *n*-butanol in the liquid phase catalysed by solid acids proceeds according to a rate equation, which is first order with respect to acetic acid and zeroth order with respect to *n*-butanol [56]. Table X shows the conversion, selectivity and rate constant for

TABLE X Catalytic activity of unmodified and modified TiO_2-SiO_2 towards the esterification of acetic acid

Sample no.	Sample code	Conversion (%)	Selectivity (%)	Rate constant ($s^{-1}\ m^{-2}$)
1	TiO_2-SiO_2, 723 K	21.66 (4)	100	1.243×10^{-7}
2	4S/TiO_2-SiO_2(H), 723 K	100 (4)	100	2.458×10^{-5}
3	2F/TiO_2-SiO_2, 723 K	22.66 (3)	100	3.282×10^{-6}
4	0.5F/4S/TiO_2-SiO_2(H), 723 K	47.05 (3)	100	2.719×10^{-5}
5	1F/4S/TiO_2-SiO_2(H), 723 K	75.36 (3)	100	2.898×10^{-5}
6	1.5F/4S/TiO_2-SiO_2(H), 723 K	78.66 (3)	100	3.553×10^{-5}
7	2F/4S/TiO_2-SiO_2(H), 723 K	90.66 (3)	100	4.000×10^{-5}
8	10F/4S/TiO_2-SiO_2(H), 723 K	78.12 (3)	100	3.909×10^{-5}
9	2F/4S/TiO_2-SiO_2(H), 383 K	73.33 (3)	100	1.631×10^{-4}
10	2F/4S/TiO_2-SiO_2(H), 623 K	99.1 (3)	100	3.218×10^{-4}
11	2F/4S/TiO_2-SiO_2(H), 823 K	42.33 (3)	100	1.078×10^{-5}
12	2F/4S/TiO_2-SiO_2(H), 923 K	4.99 (3)	100	1.231×10^{-6}

Note: (H) indicates H_2SO_4 impregnated sample prepared at pH 3. Figures in the parentheses are the reaction times in hours.

esterification of acetic acid over sulfate, fluoride, fluoride with sulfate modified and pure TiO_2-SiO_2 catalysts. Fluoride-modified sulfated TiO_2-SiO_2 mixed oxides have much higher values for rate constant than unmodified, fluoride and sulfate modified TiO_2-SiO_2 mixed oxides.

Such as esterification reaction can be catalysed by Bronsted acid sites. The mechanism involved in the reaction is as follows.

$$\begin{aligned} \mathrm{RCOOH} + \mathrm{H^+} &\Leftrightarrow \mathrm{RC^+(OH)_2} + \mathrm{R'OH} \\ &\Leftrightarrow \mathrm{RC(OH)(OH_2^+)(OR')} \\ &\Leftrightarrow \mathrm{RCOOR'} + \mathrm{H_2O} + \mathrm{H^+} \end{aligned}$$

The esterification reaction is catalysed by strong acid sites on the solid surface. As shown from sulfate content analysis (wt%), though there is a sulfate loss at 723 K, the surface sulfate concentration of fluoride-modified sulfated TiO_2-SiO_2 is more than that of sulfated TiO_2-SiO_2. So, it is observed that (Table X) the activity of fluoride-modified sulfated TiO_2-SiO_2 is higher than that of sulfated TiO_2-SiO_2 at 723 K calcination. The surface sulfate concentrations have the same trend as the activity for esterification of acetic acid. Clearly, the enhanced surface sulfate presence due to the fluoride, and a simultaneous inductive effect of sulfate and fluoride ions, accounts for enhanced activity. To support this argument another point is that fluoride-modified TiO_2-SiO_2 is less active than both the sulfated and the fluoride-modified sulfated TiO_2-SiO_2 for the reaction under identical conditions. This type of observation has also been interpreted by Huang *et al.* [57] where modification of sulfated zirconia with tungsten oxide retains the sulfate content that enhances the hexane conversion. So, modification with fluoride ions, the Bronsted acid strength of sulfated TiO_2-SiO_2 increases, resulting in higher catalytic activity for esterification reaction. Comparing this reaction with other catalysts like CeO_2-ZrO_2 [58], SO_4^{2-}/Sm_2O_3 [59], SO_4^{2-}/SnO_2 [60], SO_4^{2-}/CeO_2 [61], SO_4^{2-}/TiO_2 [62], ZrO_2 [63] and Mo-ZrO_2 [64] the fluoride-modified SO_4^{2-}/TiO_2-SiO_2 have very high values for rate constant.

The conversion increases with increase in fluoride loading but decreases with calcination temperature (in the range 723 to 923 K). The former may be due to increase in strength of Brönsted acid sites with fluoride loading over sulfated TiO_2-SiO_2 while the latter would be due to the reverse. It is also observed that the catalyst remains active after ten cycles without change in rate constant.

3. Summary

Anion modified titania-silica mixed oxide acts as a novel class of catalyst and has been widely applied in acid catalysis. Modification of the hydrous gel with anions can alter the textural as well as the acidic properties of the sample. Control of porosity and generation of new strong acid sites, which depend on the method of preparation, source and concentration of anions affect the catalytic activity of TiO_2-SiO_2 mixed oxide. The presence of anions facilitates the crystallisation at lower temperature but stabilises the anatase phase of titania at higher temperature. Dispersed fluoride ions effectively promote the thermal stability of sulfate ions. In case of 2-propanol conversion the low acetone selectivity indicates the insufficient number of redox sites. The selectivity study showed that methanol dehydration on TiO_2-SiO_2 and SO_4^{2-}/TiO_2-SiO_2 is a combination of parallel and consecutive reactions. In cumene conversion reaction, TiO_2-SiO_2 shows a better selectivity for benzene, whereas sulfated TiO_2-SiO_2 is selective for α-methyl styrene. Further, the impregnation of fluoride ions over sulfated TiO_2-SiO_2 increases the selectivity for benzene. The acid strength of 2F/4S/TiO_2-SiO_2 is more than that of PO_4^{3-}/TiO_2-SiO_2, 2F/TiO_2-SiO_2 and 4S/TiO_2-SiO_2. So the increase in acid strength is probably due to the increase in Bronsted acid sites. The acidity and porosity of the catalyst control the yield and selectivity to the mono-nitro product. Enhancement of surface sulfate presence due to fluoride ions and a simultaneous inductive effect of sulfate and fluoride ions account for the higher rate of esterification of acetic acid.

Acknowledgements

The authors are thankful to Dr. S. N. Das, Head, EM & IC Department for his constant encouragement and Dr. Vibhuti N. Misra, Director, Regional Research

Laboratory (CSIR), Bhubaneswar, for giving permission to publish this paper. One of the authors, SKS is obliged to CSIR, New Delhi for a research associateship.

References

1. K. TANABE, M. MISONO, Y. ONO and H. HATTORI, "New Solid Acids and Bases, Their Catalytic Properties Studies on Surface Science and Catalysis 51" (Kodamsha Elsevier, Amsterdam, 1989) p. 27.
2. M. ITOH, H. HATTORI and K. TAMABE, *J. Catal.* **35** (1974) 225.
3. E. I. KO and J. P. WEISSMANN, *ibid.* **105** (1987) 511.
4. H. NAKABAYASHI, *Bull. Chem. Soc. Jpn.* **65** (1992) 914.
5. J. R. SOHN and H. J. JANG, *J. Catal.* **132** (1991) 563.
6. S. IMAMURA, H. TORUMOTO and S. ISHIDA, *Ind. Eng. Chem. Res.* **28** (1989) 1449.
7. Z. LIU, J. TABORA and J. R. DAVIS, *J. Catal.* **149** (1994) 117.
8. K. TANABE, T. SUMIYOSHI, K. SHIBATA, T. KIYOURA and J. KITAGARA, *J. Bull. Chem. Soc. Jpn.* **47** (1974) 1064.
9. H. H. KUNG, *J. Solid State Chem.* **52** (1984) 191.
10. T. LOPEZ, J. NAVARRETE, R. GOMEZ, O. NOVARO, F. FIGUERAS and H. ARMENDARIZ, *Appl. Catal.* **125** (1995) 217.
11. M. HINO and K. ARATA, *J. Chem. Soc. Chem. Commun.* (1980) 851.
12. *Idem.*, *ibid.* (1979) 1148.
13. G. LARSEN, E. LOTERO, M. NABITY, L. M. PETKOVIC and D. S. SHOBE, *J. Catal.* **164** (1996) 246.
14. J. R. SOHN and H.J. JANG, *ibid.* **136** (1992) 267.
15. J. R. SOHN, H. J. JANG, M. Y. PARK, E. H. PARK and S. E. PARK, *J. Mol. Catal.* **93** (1994) 149.
16. J. NAVARRETE, T. LOPEZ and R. GOMEZ, *Langmuir* **12** (1996) 4385.
17. T. LOPEZ, P. BOSCH, F. TZOMPANTZI, R. GOMEZ, J. NAVARRETE, E. LOPEZ-SALINAS and M. E. LLANOS, *Appl. Catal. A. Gen* **197** (2000) 107.
18. K. M. PARIDA, S. K. SAMANTARAY and H. K. MISHRA, *J. Coll. Interf. Sci.* **216** (1999) 127.
19. S. K. SAMANTARAY and K. M. PARIDA, *Appl. Catal.* A **211** (2001) 175.
20. *Idem.*, *ibid.* A **220** (2001) 9.
21. *Idem.*, *React. Kinet. Catal. Lett.* **78**(2) (2003) 381.
22. W. T. MINEHAN, L. G. MESSING and C. G. PANTANO, *J. Non-Cryst. Solids* **108** (1989) 163.
23. A. J. LECLOUX, S. NONET, F. NOVILLE and J. P. PIRARD, *Ann. Chim. Fr.* **16** (1991) 75.
24. J. M. CRIADO and C. REAL, *J. Chem. Soc. Faraday Trans.* **179** (1983) 2765.
25. T. GUNJI, Y. NAGAO, T. MISONO and Y. ABE, *J. Non-Cryst. Solids* **107** (1989) 149.
26. K. NAKAMOTO, "Infrared and Raman Spectra of Inorganic and Coordination Compounds," 4th ed. (Wiley, New York, 1986).
27. G. RAMIS, G. BUSCA, V. LORENZELLI, P. F. ROSSI, M. BENSITEL, O. SAUR and J. C. LAVALLEY, in Proc. IXth Int. Congr. on Catalysis, Calgary, Canada, 1988, p. 1874.
28. A. MENNOUR, C. ECOLIVET, D. CORNET, J. F. HEMIDY, J. C. LAVALLEY, L. MARIETTE and P. ENGELHARD, *Mater. Chem. Phys.* **19** (1988) 301.
29. S. KONDO, H. YAMAGOUCHI, Y. KAJIYAMA and T. ISHIKAWA, *J. Chem. Soc. Faraday Trans.* **180** (1984) 2033.
30. A. A. TSYGANENKO, *Zh. Fiz. Khim.* **56** (1982) 2330.
31. J. B. PERRI, *J. Phys. Chem.* **69** (1965) 220.
32. T.-C. LIU and T.-J. CHENG, *Catal. Today* **26** (1995) 71.
33. B. Y. ZHAO, X. P. XU, H. R. MA, J. M. GAO, D. H. SUN, R. R. WANG and Y. Q. TANG, *Wili Huaxue Xuebao* **9** (1993) 8.
34. K. KANDORI, S. UCHIDA, S. KATAOKA and T. ISHIKAWA, *J. Mater. Sci.* **27** (1992) 719.
35. D. G. BARTON, S. L. SOLED, G. D. MEITZNER, G. A. FUENTES and E. IGLESIA, *J. Catal.* **181** (1999) 57.
36. B. H. DAVIS, R. A. REOGH and R. SRINIVASAN, *Catal. Today* **20** (1994) 219.
37. A. K. DALAI, R. SETHURAMAN, S. P. R. KATIKANENI and R. O. IDEM, *Ind. Eng. Chem. Res.* **37** (1996) 3869.
38. S. BRUNAUER, D. W. DEMMING, L. S. DEMMING and E. TELLER, *J. Amer. Chem. Soc.* **62** (1940) 1723.
39. E. P. BARRETT, L. G. JOYNER and P. P. HALONDA, *ibid.* **73** (1951) 373.
40. F. M. BAUTISTA, J. M. CAMPELO, A. GARCIA, D. LUNA, J. M. MARINAS, A. A. ROMERO, J. G. NAVIO and M. MACIAS, *J. Catal.* **145** (1994) 107.
41. P. K. PATTNAYAK and K. M. PARIDA, *J. Coll. Interf. Sci.* **226** (2000) 840.
42. A. M. TUREK, I. E. WACHS and E. DE CANIO, *J. Phys. Chem.* **96** (1992) 5000.
43. J. R. SOHN and H. J. KIM, *J. Catal.* **101** (1986) 428.
44. Y. OKAMOTO and T. IMANAKA, *J. Phys. Chem.* **92** (1988) 7102.
45. J. M. LEWIS and R. A. KYDD, *J. Catal.* **132** (1991) 465.
46. I. CARRIZOSA and G. MUNUERA, *ibid.* **49** (1977) 174.
47. T. MISHRA, K. M. PARIDA and S. B. RAO, *Appl. Catal.* A **166** (1998) 115.
48. A. N. KO and B. W. WOJCIECHOWSHI, *Prog. Rect. Kinet.* **12** (1984) 201.
49. G. WENDT, *Z. Chem.* **17** (1977) 118.
50. P. A. JACOBS, H. E. LEEMAN and J. B. UYTTERHOEVEN, *J. Catal.* **33** (1974) 17.
51. E. T. SHAO and E. J. MCINNICH, *ibid.* **4** (1965) 586.
52. B. M. CHOUDARY, M. SATEESH, M. LAKSHMI KANTAM, K. KOTESWARA RAO, K. V. RAM PRASAD, K. V. RAGHVAN and J. A. R. P. SARMA, *Chem. Commun.* (2000) 25.
53. K. M. PARIDA and P. K. PATTNAYAK, *Catal. Lett.* **47** (1997) 255.
54. T. MISHRA and K. M. PARIDA, *J. Mol. Catal.* **121** (1997) 91.
55. T. J. KWOK and K. JAYASURIYA, *J. Org. Chem.* **59** (1994) 4939.
56. S. NAMBA, Y. WAKASHIMA, T. SHIMIZU, H. MASUMOTO and T. YASHIMA (Elsevier, Amsterdam, 1989).
57. Y. Y. HUANG, B. Y. ZHAO and Y. C. XIE, *Appl. Catal.* **171** (1998) 75.
58. S. SUGUNAN and B. VARGESE, *Ind. J. Chem.* **37A** (1998) 806.
59. S. SUGUNAN and C. R. KAMAREE SEENA, *Ind. J. Chem.* **37A** (1998) 438.
60. *Idem.*, *ibid.* **37A** (1998) 669.
61. *Idem.*, *ibid.* **38A** (1999) 1123.
62. *Idem.*, *ibid.* **38A** (1999) 947.
63. K. TAKAHASHI, M. SHIBAGAKI and H. MATSUSHITA, *Bull. Chem. Soc. Jpn.* **62** (1989) 2353.
64. B. M. REDDY and V. R. REDDY, *Bull. Catal. Soc. Ind.* **9**(1/2) (1999) 48.

Received 20 May
and accepted 22 December 2003